Imaging the buried MgO/Ag interface: Formation mechanism of the STM contrast

Andrei Malashevich,[1,2,*] Eric I. Altman,[1,3] and Sohrab Ismail-Beigi[1,2,4,5]

[1]*Center for Research on Interface Structures and Phenomena (CRISP), Yale University, New Haven, Connecticut 06520, USA*

[2]*Department of Applied Physics, Yale University, New Haven, Connecticut 06520, USA*

[3]*Department of Chemical and Environmental Engineering, Yale University, New Haven, Connecticut 06520, USA*

[4]*Department of Physics, Yale University, New Haven, Connecticut 06520, USA*

[5]*Department of Mechanical Engineering and Materials Science, Yale University, New Haven, Connecticut 06520, USA*

(Received 21 July 2014; revised manuscript received 12 September 2014; published 20 October 2014)

Scanning tunneling microscopy (STM) provides real-space electronic state information at the atomic scale that is most commonly used to study materials surfaces. An intriguing extension of the method is to attempt to study the electronic structure at an insulator/conductor interface by performing low-bias imaging above the surface of an ultrathin insulating layer on the conducting substrate. We use first-principles theory to examine the physical mechanisms giving rise to the formation of low-bias STM images in the MgO/Ag system. We show that the main features of the low-bias STM contrast are completely determined by the atoms on the surface of MgO which overcomes prior ambiguities in assigning observed STM features to atomic positions of the substrate or thin film in such an epitaxial thin film system. Hence, the low-bias contrast is formed by states at the Fermi level in the Ag that propagate evanescently through the lattice and atomic orbitals of the MgO on their way to the surface. We develop a number of analysis techniques based on an *ab initio* tight-binding representation that allows identification of the origin of the STM contrast in cases where previous approaches have proven ambiguous.

DOI: 10.1103/PhysRevB.90.165426 PACS number(s): 68.37.Ef, 68.35.Ct, 71.15.Mb

I. INTRODUCTION

Metal-oxide surfaces and interfaces have been, and continue to be, a subject of significant scientific and technological interest due to the fact that metal oxides display a wide range of physical basic science phenomena that are simultaneously useful in technological applications. For example, oxide surfaces are used for catalysis or as gas sensors [1,2], oxide insulators are ubiquitous as gate insulators in transistors, and recent advances in layer-by-layer growth have triggered great activity in the study and design of oxide heterostructures [3,4]. In addition, the physical and chemical properties of metal oxides in thin-film form can differ substantially from those of their bulk forms, because these properties are affected strongly by the presence of surfaces and interfaces and especially the substrate. A classical example is provided by ultrathin films of an oxide such as MgO on a metallic substrate where electron transfer from the metal to the surface of the oxide can drive oxidation and other reactions [5].

From the viewpoint of direct characterization of oxide thin films in real space, scanning tunneling microscopy (STM) is readily able to visualize the surface of a system. A more intriguing possibility is to attempt to use STM on the surface of an oxide thin film to learn about the buried interface below the surface. If one can selectively probe the interface versus the surface by, e.g., tuning the bias voltage, one has on hand a powerful method to study interfaces at the atomic scale and in real space without the requirement of long-range order typical of diffraction-based methods [6–9].

One of the prototypical metal/oxide interfaces that has been studied extensively by using STM in the past two decades is the M/MgO interface, where M is either Mo or Ag. Let us briefly summarize the key findings about this system. Gallagher *et al.* [10] performed a scanning tunneling microscopy (STM) study on a thin MgO film grown on the (001) surface of Mo and were able to obtain STM images for MgO thicknesses up to 25 Å despite the insulating nature of MgO. Schintke *et al.* [11] performed scanning tunneling spectroscopy (STS) as well as first-principles calculations on a thin MgO film on Ag (001) and found that the STS spectrum was essentially flat for a range of bias voltages between -4 and $+1.7$ V; the first peak in the STS spectrum at 1.7 V for the thinnest films disappeared with MgO thickness whereas a peak at 2.5 V remained constant with thickness. The thickness independence permitted an identification of the 2.5 V feature with electronic states belonging to the MgO which yielded an estimated band gap of 6.5 V for MgO. The density functional theory (DFT) calculations of the local density of states (LDOS) for MgO thicknesses between 0 and 3 atomic layers in the same work found a good agreement with their experimental results. Their main conclusion was that, for bias voltages within the MgO band gap, the STM is probing Ag states through the MgO layer and that ultrathin MgO is required since the Ag wave functions decay exponentially in the insulating regions.

Lopez and Valeri [12] performed DFT calculations of the MgO/Ag (001) system for one and two layers of MgO, including several calculations with missing oxygen atoms. They calculated STM images within the Tersoff–Hamann approximation [13]. Their main conclusions were in agreement with the findings of Schintke *et al.* [11]: at low-bias voltages, the Ag states at the interface are probed whereas at high positive bias voltage the surface of MgO is probed. Within this picture, if an oxygen atom is missing at the MgO/Ag interface, one would expect to see a bright STM feature on top of the vacancy at low voltages from the Ag atom just below the vacancy, but such a bright feature was not actually

*andrei.malashevich@yale.edu

seen, a difference attributed to geometrical effects due to the relaxation of the top MgO layer.

We note that, in the case of the MgO/Ag (001) system, the MgO film is commensurate with the Ag substrate so that Mg and O atoms are in vertical registry with the Ag atoms along the (001) direction. Furthermore, the rock-salt nature of MgO ensures that cation and anion atoms in consecutive (001) atomic layers switch identity. In these conditions, assignment of observed STM features is ambiguous in theory and experiment. A typical tool used theoretically is an analysis of the projected density of states (PDOS) onto the constituent atoms. The PDOS is very useful because it directly identifies which atoms can contribute to tunneling at a given bias voltage, but unfortunately mere existence of a nonzero PDOS on some atom at a certain energy does not tell us to what extent the atomic orbitals of that atom actually contribute to the STM tunneling signal above the surface. Hence, we believe that a more detailed theoretical investigation of this model system is necessary to determine precisely what electronic states are actually being observed in the surface STM measurement.

In this work, we have used a variety of first-principles calculations and analyses to study the origin and formation of the STM signal above the surface. All results show that the STM signal at low bias (i.e., at the Fermi level) is completely dominated by the contribution of the atomic orbitals of the topmost MgO surface layer; atomic orbitals belonging to Ag atoms in the substrate make a negligible contribution. Nevertheless, since the MgO film is insulating, the states at the Fermi level that are being imaged begin in the Ag substrate, couple to the atomic orbitals of the MgO in the interfacial region, and decay evanescently through the film on their way to the surface: the coupling is best understood as being through the lattice of the MgO and its associated atomic orbitals. Unfortunately, the nature of the Ag-MgO coupling turns out to be complex and consists of interfering paths via both valence and conduction band states of the MgO film.

The body of the paper is organized as follows: Section II describes the details of our numerical simulations. Then the main results are presented in Sec. III. The results are further analyzed by using a simplified tight-binding model in Sec. IV. The key findings are summarized in Sec.V where we also provide our outlook for future work in this general area.

II. COMPUTATIONAL METHODS

Our first-principles calculations use DFT within the generalized-gradient approximation (GGA) of Perdew and Wang (PW91) [14]. We employ a plane-wave pseudopotential approach utilizing Vanderbilt ultrasoft pseudopotentials [15] as implemented in the QUANTUM ESPRESSO software package [16]. The atomic configurations and cutoff radii used for pseudopotential generation are shown in Table I. For Ag and Mg atoms, nonlinear core corrections are employed [17]. The plane-wave kinetic energy and charge density cutoffs are 35 and 280 Ry, respectively. Supercells in the form of two-dimensional slabs are constructed with three monolayers (MLs) of face-centered cubic Ag with (001) surface orientation and various thicknesses of rock-salt MgO. Below, we label the MgO thickness by the number of MLs (atomic planes) comprising the film. The supercells contain a vacuum region

TABLE I. Pseudopotential reference valence configurations and corresponding cutoff radii (atomic units).

Atom	Valence configuration	r_c^s	r_c^p	r_c^d
Ag	$4d^{10}5s^{1}5p^{0}$	2.5	2.5	2.1
Mg	$2p^{6}3s^{1}3p^{0.75}3d^{0}$	2.3	2.0	2.0
O	$2s^{2}2p^{6}$	1.2	1.2	

of at least 20 Å that separates each slab from its periodic images. In addition, to ensure the absence of long-ranged electrostatic interactions between the periodic slabs, we use the dipole correction technique [18] to eliminate any electric field in the vacuum region entirely.

For a primitive interfacial unit cell that simulates MgO epitaxial to the Ag substrate (Fig. 1), a 12×12 k-point sampling of the two-dimensional Brillouin zone is employed. Equivalent meshes of k points are used for larger supercells. The Brillouin zone integration is performed by using the Gaussian smearing method with a smearing width of 2 mRy. We also have examined several other smearing methods and verified that for reasonable choices of smearing widths (equivalently temperatures), the density of states and location of the Fermi level do not depend on the details of the smearing method (see Appendix A for further details). For STM simulations, we use the Tersoff–Hamann approximation [13]. The main focus of the present work is on low-bias STM analysis for which Tersoff–Hamann approximation is an appropriate choice. Specifically, since at low bias the STM current is proportional to the LDOS at the Fermi level E_F, we will be using the theoretically calculated LDOS as a surrogate for the STM signal and will use the two terms interchangeably.

In Sec. IV we construct a tight-binding description of the MgO/Ag system. The atomic orbitals comprising the tight-binding basis are those included in the pseudopotential generation and are listed in Table I. In this basis, we compute matrix elements of the Kohn–Sham Hamiltonian as well as

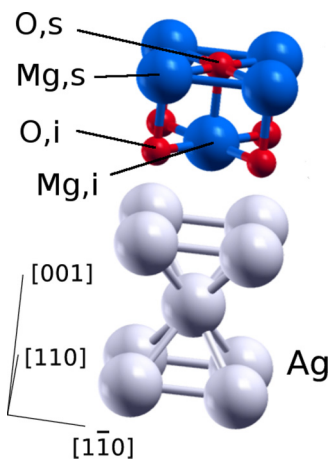

FIG. 1. (Color online) The unit cell describing two MLs of MgO on top of three MLs of Ag (001): "i" means "interface" and "s" stands for "surface." The in-plane [110] and [1$\bar{1}$0] directions are labeled as is the out-of-plane [001] direction.

the atomic orbital overlap matrices. This starting basis is normalized but not orthogonal (orbitals on different atoms have nonzero overlap). In certain parts of the analysis in Sec. IV, it is helpful to have an orthonormal atomic orbital basis: we use the Löwdin transformation to arrive at an equivalent set of orthonormal Löwdin orbitals [19]. Finally, all PDOS calculations in this work employ Löwdin orbitals for the projections.

III. RESULTS

A. Bulk Ag and MgO

Our computed lattice constants of bulk fcc Ag and rock-salt MgO are $a_{Ag} = 4.13$ Å and $a_{MgO} = 4.26$ Å in good agreement with the respective experimental values [20] of 4.09 Å and 4.21 Å. Since these lattice parameters match to within 3%, epitaxial growth of MgO thin films on Ag (001) is feasible [11].

For MgO, our computed Kohn–Sham energy gap is 4.4 eV which is much smaller than the experimental value of 7.9 eV [21]: the band-gap underestimation of DFT is a well-known limitation of the theory [22,23]. However, this problem is not crucial for our study since the focus is on the low-bias range about the Fermi level, we only need to ensure that the MgO is an insulator whose band edges are well separated from the Fermi level, which is the case as shown below. For reference, we show the density of states (DOS) and atomic PDOS for bulk MgO in Fig. 2(a). As expected for an ionic oxide, the figure shows that the valence band edge is dominated by anionic O $2p$ states while the conduction band is primarily a mixture of cationic Mg $3s$, $3p$, and $3d$ states.

At the lowest approximation level, STM probes the states between the Fermi level and the bias voltage with more weight on the upper side of the energy range [24]. For insulating MgO, the natural expectation is that for low-bias voltages no electronic states of the MgO itself will be probed since the Fermi level is solidly in the band gap. Any STM image on the MgO surface must therefore originate in some way from the Ag substrate buried under the MgO film. On the other hand, for large bias voltages (positive or negative), the Fermi level will enter the energy bands of the MgO film and a large signal should be observed coming from the MgO surface itself: for large positive bias within the conduction band, Mg atoms should dominate as bright spots in the STM. Conversely, for large negative bias in the valence band, the surface O atoms should dominate the STM image.

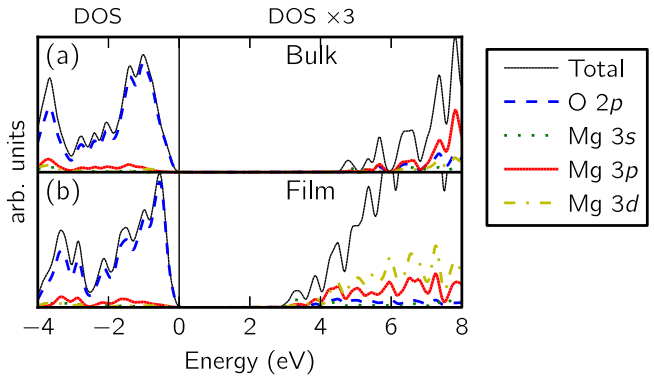

FIG. 2. (Color online) Total (DOS) and projected density of states (PDOS) of (a) bulk MgO and (b) a two-ML free-standing MgO film in vacuum. The energy is referenced to the top of the valence band indicated by the vertical black line at zero energy. To help visualize the conduction-band states, DOS and PDOS are multiplied by a factor of three for energy above zero.

TABLE II. Calculated relaxed geometry for two MLs of MgO on Ag (001). All coordinates are in Å, "i" stands for "interface" and "s" stands for "surface." "Ag" refers to the interfacial silver atom (see Fig. 1), and $z_{Ag} - z_{Ag,bulk}$ describes the vertical relaxation of the interfacial Ag compared to its bulk unreconstructed position on the surface.

	This work	Previous theory
$z_{Ag} - z_{Ag,bulk}$	−0.05	−0.06[a]
$z_{O,i} - z_{Ag}$	2.68	2.47[a], 2.73[b]
$z_{Mg,i} - z_{Ag}$	2.67	2.45[a]
$z_{O,s} - z_{Mg,i}$	2.21	2.20[a]
$z_{Mg,s} - z_{O,i}$	2.17	2.14[a]

[a]Reference [12].
[b]Reference [25].

B. Two-monolayer MgO on three-monolayer Ag(001)

Next, we studied an epitaxial ultrathin MgO film (two MLs) on the silver substrate (three MLs). The unit cell for this calculation is shown in Fig. 1 as is the final relaxed configuration: the O atoms are directly above Ag atoms, a configuration that is energetically more favorable than the alternative alignments (such as placing Mg on top of Ag). The structural parameters of the two bottom silver layers were fixed to the bulk values, while the coordinates of the MgO atoms and the interfacial Ag were fully relaxed (within the epitaxial constraint). Numerical coordinate data on the relaxed structure is displayed in Table II. Our tabulated results are in agreement with the theoretical study of Lopez *et al.* [12], aside from the substrate-overlayer distance $d \equiv z_{O,i} - z_{Ag}$ which in our case is about 0.2 Å larger than theirs. However, Giordano *et al.* [25] found a substrate-overlayer distance $d = 2.73$ Å in this system which is very similar to our result. Unfortunately, as we show below, the detailed STM image depends strongly on the precise value of d which serves as a caution to blind comparison to experiment without careful benchmarking in this specific system. We describe the reason for the d dependence in Sec. IV.

To examine the electronic structure of this interfacial system and the resulting STM image, it is fruitful to consider in parallel the isolated subsystems: a two-ML MgO thin film in vacuum and an isolated Ag substrate (three MLs) in vacuum. For these systems, the atomic coordinates are fixed at those derived from the relaxation of the original interfacial system. Figures 2(a) and 2(b) compare the DOS and PDOS for bulk MgO and the MgO thin film. We note that the band gap of the MgO film (3.0 eV) is smaller than the bulk (4.4 eV), a result consistent with previous calculations as well as experimentally observed band-gap reduction in a thin film compared to bulk [11]. By comparison, Fig. 3 shows the PDOS of the MgO subsystem in the actual MgO/Ag interfacial system: the PDOS in the

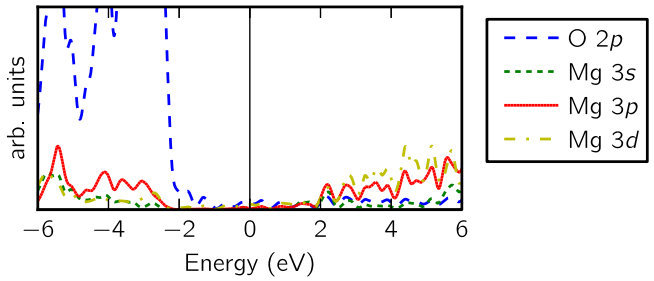

FIG. 3. (Color online) PDOS on MgO atomic orbitals of the two-ML MgO/Ag interfacial system. Energies are referenced to the Fermi level which is set to zero energy.

MgO subsystem is now nonzero in the band gap region of the free-standing MgO film, and specifically nonzero PDOS develops at the Fermi level due to the coupling to the Ag substrate. This result already hints at the fact that states in the MgO may play a role in the formation of the STM image.

We now proceed to the calculated STM images for this system. Throughout this manuscript and unless noted otherwise, we provide and discuss constant-height STM images. We have checked that, qualitatively, constant-height and constant-density images look quite similar (see Appendix B). The STM images in this work are computed at 1 Å above the surface. This is much smaller than typical experimental surface-tip separation of 5–8 Å. The reduction of the surface-tip distance in simulations based on Tersoff–Hamann approximation is a known limitation that arises from the numerical difficulties associated with computing an exponentially small local density of states in the rapidly decaying tail region of this function away from the surface [26]. In our case, the STM images can be simulated well for heights of 1–2 Å above the surface, while for larger heights numerical noise distorts the image significantly (see Appendix C for examples). Therefore, we choose a surface-tip distance of 1 Å to describe high-quality images.

The STM image (LDOS at E_F) for the bare Ag (001) surface is shown in Fig. 4(a): not surprisingly, the bright spots correspond to the locations of the silver atoms on the surface layer and follow the square pattern of the surface lattice. The STM image for the relaxed MgO/Ag system is shown in Fig. 4(b): the brightest spots in the STM image are at the location of the surface O atoms with weaker features at the Mg locations. In Fig. 4(c), we show the result for three ML of MgO on Ag (001): the bright features continue to track the positions of the surface O atoms, and the overall image simply looks like a translated version of the two-ML result of Fig. 4(b). We also note that, when we calculate the STM image of the bare Ag (001) surface at the same height above the top Ag atoms as in the two-ML MgO/Ag calculation, we obtain essentially a null result: the maximum density is smaller by a factor of 10^2 than the maximum density in Fig. 4(b) and there is almost no contrast. In addition to the in-plane shift of the image, the overall intensity of the STM image for three MLs is smaller than for two MLs due to the exponential decay of the states at the Fermi level through the MgO film, a fact we have verified by studying a range of thicknesses from two to eight MLs of MgO. Since the Ag is obviously crucial to having states at the Fermi level, and yet the STM image tracks the position of the surface atoms of the insulator, a satisfactory explanation for low-bias observations is lacking and motivates further analysis and computations below.

These STM images do not agree with those given by Lopez *et al.* [12] who observed bright spots at locations on top of the surface Mg atoms which vertically overlap the interfacial Ag atoms in the two-ML MgO case. However, there is no great cause for concern due to the strong overlayer-substrate separation d dependence of the STM results. In Fig. 5(b) we show the STM image computed by using d fixed at the value taken from Ref. [12]. The STM image in this case now resembles their result with bright spots at the surface-Mg locations.

Comparing the results shown in Fig. 4 to experimental STM images [11] or atomic force microscopy results [27], we find that any of the panels of Fig. 4 agree with experiments because all the images show the square pattern with periodicity of the Ag (001) substrate. Therefore, we again emphasize the need for our more thorough theoretical investigation below that elucidates the origin of observed STM features.

Before ending this section, we briefly describe some high-bias-voltage results for the Mg/Ag system. We simulated the STM image at 3 V bias for MgO thickness of 1, 2, 3, 4, 8, and 16 MLs. The STM features are always located at the positions of the Mg atoms on the topmost layer, and starting at two MLs,

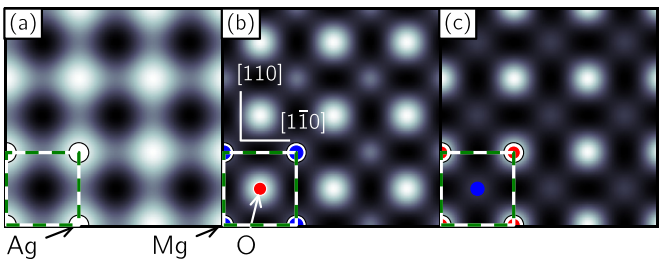

FIG. 4. (Color online) Constant-height near-zero-bias STM simulations of surfaces of (a) Ag (001), (b) two-ML MgO/Ag(001), and (c) three-ML MgO/Ag(001). The images are computed at 1 Å above the surfaces. The blue (red) circles denote the positions of Mg (O) atoms at the surface monolayer. The white circles denote positions of Ag atoms of the interfacial layer. The dashed squares outline the unit cell used in these calculations.

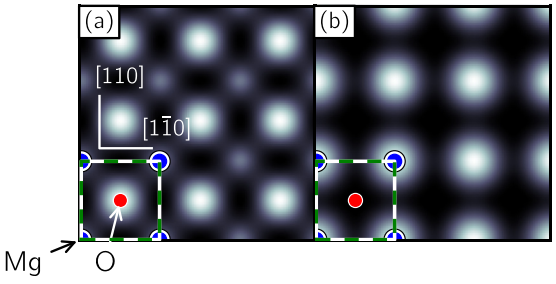

FIG. 5. (Color online) Dependence of STM images on the overlayer-substrate distance d for two-ML MgO/Ag (001). (a) is based on our theoretically relaxed structure with $d = 2.68$ Å and is identical to Fig. 4(b). (b) uses d fixed to 2.47 Å. STM images are computed at 1 Å above the surfaces. The blue (red) circles denote the positions of Mg (O) atoms at the surface monolayer. The dashed squares outline the unit cell used in the calculations.

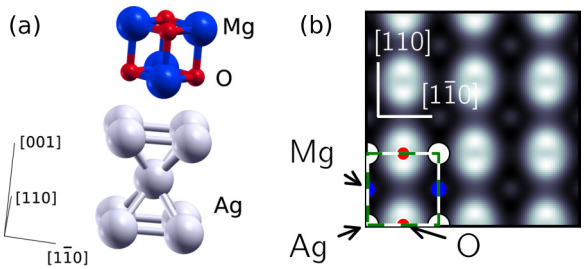

FIG. 6. (Color online) (a) Side view of the two-ML MgO/Ag(001) system with the MgO overlayer shifted horizontally in the [110] direction by half of the unit cell from its relaxed position. (b) Corresponding constant-height near-zero-bias STM image simulated at 1 Å above the surface. The blue (red) circles denote the positions of Mg (O) atoms at the surface monolayer. The white circles denote positions of Ag atoms at the interfacial layer. The dashed squares outline the unit cell used in the simulation.

the STM image intensity does not show any dependence on the MgO thickness. Combined with the PDOS results in Fig. 2, we conclude that, as noted previously [12], the high-bias-voltage STM probes the Mg-derived conduction bands of the MgO film itself. We note that, even though the Tersoff–Hamann approximation is not very well justified for high-bias voltages, it yields a physically reasonable and qualitatively correct result for this system.

C. Overlayer shift

In a next step, we consider "sliding" the MgO layer with respect to the Ag substrate. In particular, starting from the original unit cell shown in Fig. 1, we shift the MgO overlayer by half of the unit cell in the [110] direction. In the resulting structure shown in Fig. 6(a), the in-plane coordinates of the MgO atoms do not coincide with the Ag ones. The resulting low-bias STM image shown in Fig. 6(b) clearly indicates that the bright spots in the STM image move together with the overlayer atoms (O atoms in particular) with no visible features at the positions of the Ag atoms.

We note that there exists an interesting splitting of the bright spots on top of surface O atoms in Fig. 6(a), a feature that is not present in Fig. 4(b). The appearance of this splitting may be due to the increased importance of the O $2p_x$ and $2p_y$ orbitals in the STM image formation. As we show in Sec. IV, when MgO is in its relaxed configuration with respect to the Ag substrate, the bright spots on top of O atoms are formed mainly by O $2p_z$ orbitals. When the overlayer is shifted relative to the substrate, the overlap between O $2p_z$ and Ag orbitals in the second Ag layer from the interface is substantially reduced. This qualitative argument may explain why the role of O $2p_z$ orbital is diminished and O $2p_x$ and $2p_y$ become more important. However, a more thorough study, beyond the scope of this work, is needed to give a satisfactory explanation for this splitting phenomenon.

D. Incommensurate overlayer

To further elucidate the origin of the STM features in MgO/Ag system at low-voltage bias, we construct a number of simulation cells where the relative in-plane registry of the MgO and Ag atoms varies across the unit cell which allows us

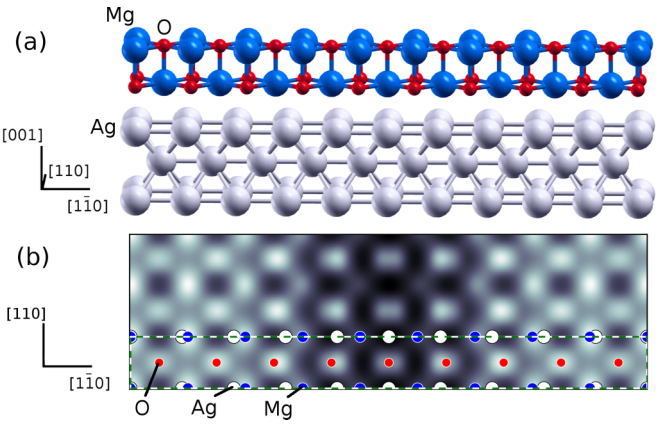

FIG. 7. (Color online) (a) Side view of the two-ML MgO/Ag(001) system with the MgO overlayer stretched horizontally. (b) Corresponding constant-height near-zero-bias STM image. The dashed rectangle outlines the unit cell used in the simulation.

to directly examine the effect of the relative alignment of the two materials on the STM image in a single calculation.

We consider a supercell which is elongated to contain ten primitive lattice vectors of the bulk Ag substrate in the horizontal direction. We then uniformly stretch a two-ML-thick MgO film which is nine unit cells long in the horizontal direction to lie on top of the ten unit cells of Ag (tensile strain). Note that this structure is a theoretical construction used to perform a "gedanken experiment" to elucidate the STM image formation mechanism. Therefore, to avoid complications in analysis, we do not perform any structural relaxations and keep all vertical coordinates fixed to the values quoted in Table II when computing STM images. (Nevertheless, we have explicitly verified that if we permit for structural relaxations, the atomic positions in the MgO layer change at most by 0.1 Å and there are no significant changes in the computed STM images.)

The resulting structure is shown in Fig. 7(a) along with the resulting STM image in Fig. 7(b). If the Ag atoms dominated the STM current at low bias, we would expect to see bright features with the periodicity of the Ag substrate which is clearly not the case. Instead, the maxima of the LDOS at E_F track the periodicity of the MgO overlayer. In addition, there is an overall Moiré-like modulation of the brightness that indicates the presence of interference between various contributions to the final STM image. The Moiré pattern is brightest in places where the MgO overlayer is in registry with the substrate—when the interfacial O atoms lie close to the the interfacial Ag atoms. Similar Moiré patterns have been observed experimentally in STM images of mismatched oxide layers on metal surfaces. Because it is not possible to unambiguously distinguish topographic from electronic contrast in STM images, the contrast in these experiments may be due to a rumpling of the oxide layer as it moves in and out of registry with the substrate or due to a change in coupling of the oxide layer to the metal as the registry varies [28,29].

In an attempt to separate the role of each of the two MgO monolayers, we performed a new calculation where we stretched only the atomic plane in contact with the Ag substrate while keeping the MgO layer on the surface in registry with the Ag substrate. The resulting structure and STM image are

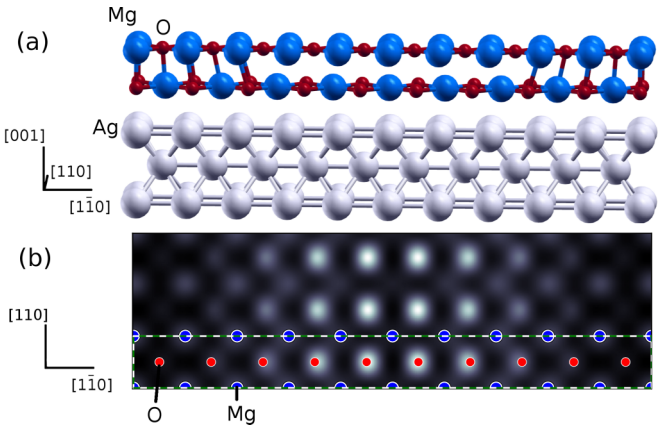

FIG. 8. (Color online) (a) Side view of the two-ML MgO/Ag(001) system with only the interfacial MgO layer stretched horizontally. (b) Corresponding constant-height near-zero-bias STM image. The dashed rectangle outlines the unit cell used in the simulation.

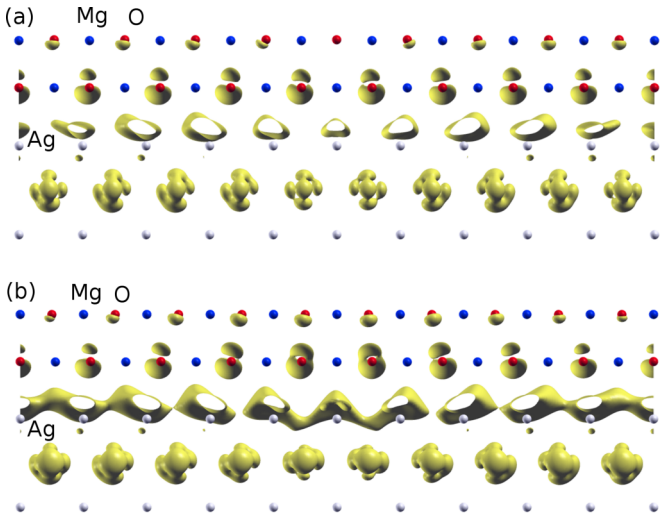

FIG. 9. (Color online) Local density of states at the Fermi level for the structures shown in Figs. 7(a) and 8(a). The isosurface is shown at ∼10% of the maximum value of the function.

shown in Figs. 8(a) and 8(b). In this case, the bright STM features have the periodicity of the top MgO layer, but the location of the brightest features change between Mg and O surface atoms as a function of the horizontal coordinate.

Broadly speaking, the above two calculations provide the following picture: The STM image is formed from some nontrivial hybridization of the Ag with the Mg and O atoms in the interfacial region. The hybridization is significant even when the Mg and O atoms are out of registry with the Ag atoms, but the brightest STM images occur when the atoms are in registry because one would expect in such a case a maximized overlap of atomic orbitals between Ag and MgO. We now examine each of two results in more detail.

We consider more closely the structure shown in Fig. 7(a). In the left corner of the unit cell, we have an interfacial O atom placed directly above the interfacial Ag atom, and the surface Mg atom is above the interfacial O atom. This represents a case of maximum overlap of atomic orbitals which leads to the brightest features in the STM image of Fig. 7(b). On the other hand, in the center of the unit cell there are no Mg or O atoms directly on top of the Ag atoms which diminished overall STM brightness. In addition, the surface O atoms appear brighter in the central location which indirectly highlights their relative importance in forming the STM image. However, the intensity pattern is formed via a complex interaction in the interfacial region: the brightest features in Fig. 8(b) occur in the center of the unit cell where the surface O atoms are located directly above the Ag atoms in the *second* layer from the silver surface and there are no other atoms in between. This foreshadows the fact that a straightforward analysis of the Ag to MgO coupling that leads to the STM features is a complex undertaking.

To illustrate the importance of the oxygen sublattice in the formation of the LDOS at E_F and hence the STM image, we display three-dimensional isosurface plots of the LDOS at E_F in Fig. 9 for the two structures discussed in this section. Inside the MgO, we see primarily a decaying evanescent behavior localized on the oxygen sublattice dominated by O $2p_z$ orbitals. What this figure makes completely clear is that that the propagation of the evanescent states throughout the MgO is through the tight-binding orbitals of the MgO lattice and not as free-electron-like states originating at the Ag surface. Based on this finding, we will be performing a more thorough analysis of the MgO/Ag system by using a tight-binding representation.

IV. TIGHT-BINDING MODEL

While direct first-principles computation of the STM image (LDOS at E_F in our case) is the final theoretical output that may be compared with experiment, the mechanism that leads to the formation of the STM image on the surface is difficult to tease out from such direct computations of the final result. For example, it is difficult to simply and selectively "turn off" the contribution of certain atoms to the STM image without changing their mutual couplings or couplings to other atoms (or vice versa). A tight-binding description, on the other hand, allows one to answer a number of questions of this variety by providing a number of additional analysis opportunities.

We construct a tight-binding model of the MgO/Ag system as follows: Starting with the relaxed two-MgO/Ag system, we perform a self-consistent-field calculation while sampling the Brillouin zone on a fine 24×24 mesh of $\mathbf{k}$ points (the high density of $\mathbf{k}$ points is necessary for a smooth Fourier interpolation of the band structure in the Löwdin basis). Armed with the Hamiltonian and overlap matrices at each $\mathbf{k}$ point, $H^{\mathbf{k}}_{\alpha\beta}$ and $S^{\mathbf{k}}_{\alpha\beta}$, where Greek letters label atomic orbitals in one unit cell, we Fourier transform them to find a real-space tight-binding description. For example, the real-space Hamiltonian $h^{\mathbf{R}}_{\alpha\beta}$ is computed via

$$h^{\mathbf{R}}_{\alpha\beta} = \frac{1}{N_k} \sum_{\mathbf{k}} H^{\mathbf{k}}_{\alpha\beta} e^{-i\mathbf{k}\cdot\mathbf{R}},$$

where N_k is the total number of $\mathbf{k}$ points ($24^2 = 576$ in this case) and $\mathbf{R}$ is a lattice vector. (An analogous formula connects $S^{\mathbf{k}}$ to $s^{\mathbf{R}}$.) The matrix element $h^{\mathbf{R}}_{\alpha\beta}$ is that between orbital α in the "home" unit cell at the origin to orbital β in the unit cell centered at position $\mathbf{R}$. Diagonal elements $h^0_{\alpha\alpha}$ are the on-site

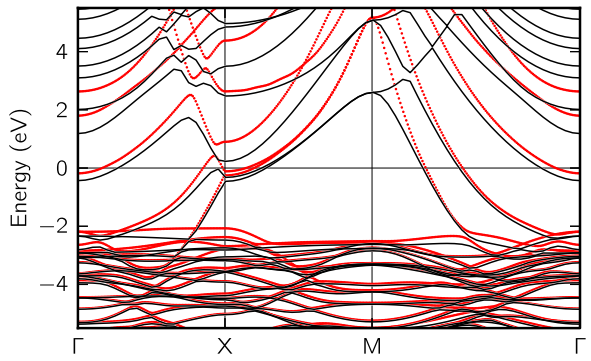

FIG. 10. (Color online) Band structure versus in-plane wave vector $\mathbf{k}$ for two MLs of MgO on Ag (001). (Black) solid lines show the plane-wave-basis band structure and (red) dotted lines show the tight-binding band structure. The Fermi level is placed at 0 eV.

energies of the orbitals. While it is generally preferable to use a tight-binding basis formed from maximally localized Wannier functions [30] which automatically guarantees orthonormality, compactness, and exact representation of the Hilbert subspace of interest, the procedure to generate such Wannier functions is extremely difficult (and was abandoned) for this material system due to the very large spread of the Mg atomic orbitals described below. Finally, we use Fourier interpolation to generate $H^{\mathbf{k}}$ at an arbitrary $\mathbf{k}$ point not in the original grid:

$$H^{\mathbf{k}}_{\alpha\beta} = \sum_{\mathbf{R}} h^{\mathbf{R}}_{\alpha\beta} e^{i\mathbf{k}\cdot\mathbf{R}}$$

(and analogously for getting $S^{\mathbf{k}}$ from $s^{\mathbf{R}}$). Solving the generalized eigenvalue problem to find the energy bands $E_{n\mathbf{k}}$,

$$\sum_{\beta} H^{\mathbf{k}}_{\alpha\beta} C^{\mathbf{k}}_{\beta n} = E_{n\mathbf{k}} \sum_{\beta} S^{\mathbf{k}}_{\alpha\beta} C^{\mathbf{k}}_{\beta n},$$

we generate the electronic band structure within our tight-binding model.

The resulting band structure for two-ML MgO/Ag is shown in Fig. 10 together with the original plane-wave-basis band structure. The tight-binding basis provides a good quantitative description of the valence bands as well as the bands that are at or near the Fermi energy. The degradation in quality above the Fermi level is normal and expected of a method based on localized orbitals once the eigenstates contain significant delocalized plane-wave character, which is the case in the conduction band at high energies. As we are focused on the states at or near the Fermi level, which form the low-bias STM image, the present tight-binding approach is deemed sufficient for continued analysis.

We use the tight-binding model to compute the STM image by computing the LDOS at E_{F} at point $\mathbf{r}$:

$$L(\mathbf{r}, E_{\mathrm{F}}) = \sum_{n,\mathbf{k}} w(E_{\mathrm{F}} - E_{nk}) |\psi_{nk}(\mathbf{r})|^2,$$

where the window function $w(E_{\mathrm{F}} - E_{nk})$ selects the states $|\psi_{nk}\rangle$ with energies E_{nk} in the vicinity of the Fermi level E_{F} (for the purpose of computing the STM images shown below, we used the window function selecting the states at $E_{\mathrm{F}} \pm 0.1$ eV). The Bloch state $\psi_{nk}(\mathbf{r})$ is expanded in the basis of atomic orbitals $\phi_\alpha(\mathbf{r})$ via

$$\psi_{n\mathbf{k}}(\mathbf{r}) = \frac{1}{\sqrt{N_k}} \sum_{\mathbf{R},\alpha} C^{\mathbf{k}}_{\alpha n} e^{i\mathbf{k}\cdot\mathbf{R}} \phi_\alpha(\mathbf{r} - \mathbf{R}). \quad (1)$$

Written explicitly in terms of the expansion coefficients $C^{\mathbf{k}}_{\alpha n}$ and atomic orbitals,

$$L(\mathbf{r}, E_{\mathrm{F}}) = \frac{1}{N_k} \sum_{n,\mathbf{k}} w(E_{\mathrm{F}} - E_{nk}) \left| \sum_{\alpha,\mathbf{R}} C^{\mathbf{k}}_{\alpha n} \phi_\alpha(\mathbf{r} - \mathbf{R}) \right|^2. \quad (2)$$

By using the atomic orbitals $\phi_\alpha(\mathbf{r})$ used in the generation of the pseudopotentials together with the energies $E_{n\mathbf{k}}$ and coefficients $C^{\mathbf{k}}_{\alpha n}$ from the tight-binding model, we can compute the LDOS at E_{F} for any point $\mathbf{r}$ above the surface and thus compute an STM image based on tight-binding theory.

The LDOS computed with Eq. (2) will always be an approximation to the more exact answer given by the computation of $\psi_{n\mathbf{k}}(\mathbf{r})$ using plane waves, and so the main question is to what extent we can use the LDOS from the tight-binding model to understand the electronic behavior of the system. Figure 11(a) shows the LDOS at E_{F} for two-ML MgO/Ag system based on Eq. (2). One can see that qualitatively it looks very similar to the image shown in Fig. 4(b), and this means that the atomic orbital basis is complete enough in the regions of interest above

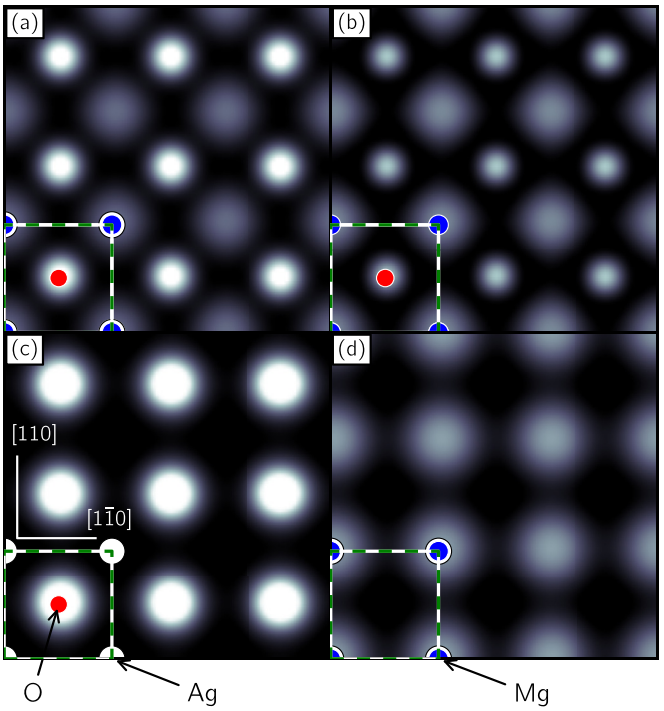

FIG. 11. (Color online) Constant-height LDOS simulations of the two-ML MgO/Ag(001) system based on the atomic-orbital tight-binding model and selective omission of orbitals in the computation of the LDOS at E_{F} in Eq. (2): (a) all orbitals included, (b) orbitals of all Ag atoms omitted, (c) orbitals of the surface Mg omitted, and (d) orbitals of the surface O omitted. All images are computed at 1 Å above the surface. The blue (red) circles denote the positions of Mg (O) atoms on the surface layer. The white circles denote positions of Ag atoms at the interfacial layer. The dashed squares outline the unit cells used in the calculations.

the surface to generate STM images that match the plane-wave results in terms of key features and brightness ratios. This encourages us to use this tool for further analysis.

One advantage of having a tight-binding model is the ability to separate contributions from different orbitals to the STM image. For example, Figure 11(b) shows the LDOS at E_F from Eq. (2) where all coefficients $C^{\mathbf{k}}_{\alpha n}$ appearing in that equation that correspond to atomic orbitals on all Ag atoms are set to zero. The fact that the image is hardly changed from the case that includes all orbitals [Fig. 11(a)] unambiguously proves that the STM contrast is formed by electronic states inhabiting the orbitals of the MgO. Next, we can zero contributions from selected surface atoms and observe changes in the STM image. Figure 11(c) shows the LDOS at E_F when surface Mg orbitals are omitted, and Fig. 11(d) shows the resulting image when surface O orbitals are omitted. Clearly, the strong changes in the images show that the surface atoms dominate the STM image formation. Furthermore, we note that omitting the Mg orbitals increases the overall brightness—this points out the fact that the final STM image is formed by a superposition of mainly destructively interfering contributions from the Mg and O sublattice above the surface.

Applying the above methodology to the case where the MgO/Ag separation d is fixed at 2.47 Å, we obtain the image shown in Fig. 12(d) which, again, is in agreement with the plane-wave result of Fig. 5(b) [for convenience, Fig. 11(a) is reproduced in Fig. 12(c) along with the plane-wave STM simulations in panels (a) and (b)]: the Mg sites become much brighter. The tight-binding method is thus able to reproduce the d dependence of the STM contrast and can be used to understand why this happens, as detailed below.

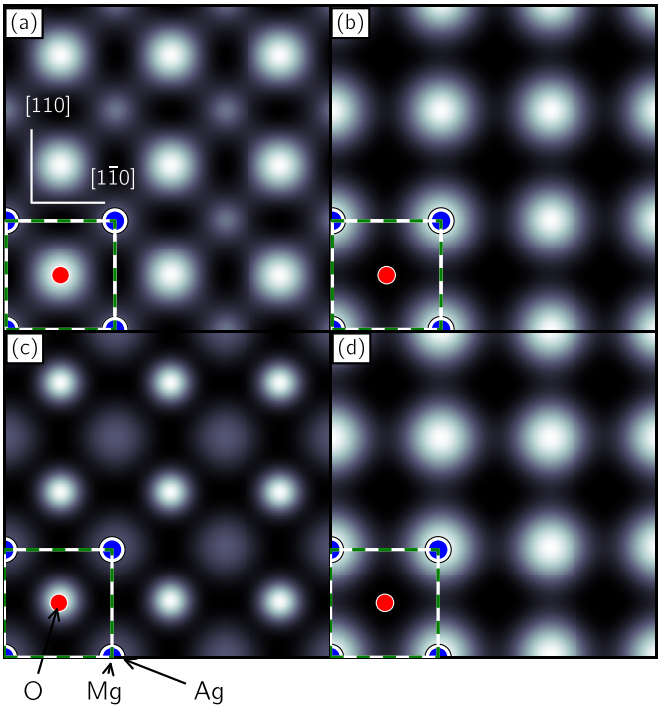

FIG. 12. (Color online) Constant-height LDOS simulations based on the plane-wave theory [panels (a) and (b)] and the tight-binding model [panels (c) and (d)] for the two-ML MgO/Ag(001) system. Panels (a) and (c) correspond to a relaxed geometry of the interface with MgO/Ag separation distance $d = 2.68$ Å, while panels (b) and (d) correspond to fixed $d = 2.47$ Å. The images are computed at 1 Å above the surface. The blue (red) circles denote the positions of Mg (O) atoms at the surface monolayer. The white circles denote positions of Ag atoms at the interfacial layer. The dashed squares outline the unit cells used in the calculations.

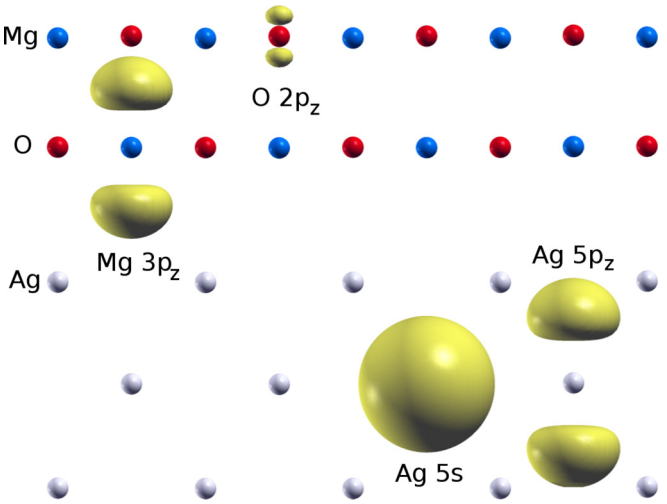

FIG. 13. (Color online) Isosurfaces of the square of the wave functions for the atomic orbitals of the Mg $3p_z$, O $2p_z$, Ag $5s$, and Ag $5p_z$ states. The isosurfaces are shown for ~60% of their respective maximum values.

The next step in the analysis of the STM image formation is to begin further examination of the strength and nature of the Ag to MgO coupling across the interface. First, we examine the relevant length scales by examining the sizes of the atomic orbitals in this system. Figure 13 shows isosurfaces of some of the important atomic orbitals on Ag, Mg, and O atoms. While the O $2p$ orbitals are quite localized, the Ag and Mg orbitals are quite extended in space: although the interfacial O and Ag atoms are closest at the interface, the Ag to Mg tight-binding matrix elements must in fact be quite sizable as well given the extent of these atomic states; appreciable matrix elements can also be expected between the interfacial Ag and the top MgO layer. These large sizes foreshadow the difficulties that will present themselves in any simple-minded analysis of the cross-interface coupling in terms of nearest neighbors and atomic arrangements localized at the interface. A secondary implication is that although the LDOS at E_F isosurface plots in Figs. 9(a) and 9(b) seem to show only O $2p$ contributions in the MgO, this is in some ways deceptive because the compact O $2p$ orbitals have high probability densities that dominate the LDOS in real space. The much-more delocalized Mg orbitals may have significant weight in the wave function but this is not visible unless one examines much smaller values of the LDOS function in real space. The importance of the Mg orbitals is discussed in more detail below.

We now switch to the Löwdin representation of orthonormal atomic orbitals to aid in simplifying the analysis: in the Löwdin basis, the overlap matrices are identity by construction so we only have to consider the Hamiltonian matrix and its orthonormal eigenvectors. We denote the Hamiltonian matrix at wave vector $\mathbf{k}$ in the Löwdin representation as $\tilde{H}^{\mathbf{k}}_{\alpha\beta}$ which

we decompose into sub-blocks corresponding to the Ag and MgO subsystems as

$$\tilde{H}^{\mathbf{k}} = \begin{pmatrix} \tilde{H}^{\mathbf{k}}_{mm} & \tilde{H}^{\mathbf{k}}_{mi} \\ \left(\tilde{H}^{\mathbf{k}}_{mi}\right)^{\dagger} & \tilde{H}^{\mathbf{k}}_{ii} \end{pmatrix},$$

where mm labels the metallic Ag subsystem, ii labels the insulating MgO subsystem, and mi labels the metal-to-insulator coupling elements. The metallic subsystem Hamiltonian $\tilde{H}^{\mathbf{k}}_{mm}$ has states at E_{F} while the insulating one $\tilde{H}^{\mathbf{k}}_{ii}$ has an energy gap at E_{F}: the coupling $H^{\mathbf{k}}_{mi}$ is responsible for creating evanescent states at energy E_{F} that propagate in the insulator.

Armed with this representation, we can first examine the nature of the states at E_{F} that propagate in the MgO. For the subspace of MgO orbitals, the eigenstates of $\tilde{H}^{\mathbf{k}}_{ii}$ form a complete basis of valence and conduction bands, so we may ask how the density of states at E_{F} is decomposed into these two subspaces. Letting $P^{\mathbf{k}}_{v}$ and $P^{\mathbf{k}}_{c}$ be orthogonal projectors onto the valence and conduction bands of the insulating MgO subsystem at wave vector $\mathbf{k}$, respectively, we compute the projected densities of states at E_{F} onto the MgO bands via

$$L_{v}\left(E_{\mathrm{F}}\right) = \frac{1}{N_k}\sum_{n,\mathbf{k}} w\left(E_{\mathrm{F}} - E_{nk}\right)\langle\psi_{n\mathbf{k}}|P^{\mathbf{k}}_{v}|\psi_{n\mathbf{k}}\rangle$$

and

$$L_{c}\left(E_{\mathrm{F}}\right) = \frac{1}{N_k}\sum_{n,\mathbf{k}} w\left(E_{\mathrm{F}} - E_{nk}\right)\langle\psi_{n\mathbf{k}}|P^{\mathbf{k}}_{c}|\psi_{n\mathbf{k}}\rangle.$$

The total density of states at E_{F} is

$$D\left(E_{\mathrm{F}}\right) = \frac{1}{N_k}\sum_{n,\mathbf{k}} w\left(E_{\mathrm{F}} - E_{nk}\right)\langle\psi_{n\mathbf{k}}|\psi_{n\mathbf{k}}\rangle.$$

The second row of Table III shows these quantities for the relaxed two-ML MgO/Ag system ($d = 2.68$ Å). We see projections for the states at E_{F} on both valence and conduction bands, and in fact the weight on the Mg-dominated conduction bands is higher than that of the O-dominated valence bands. These results show that there are at least two independent,

TABLE III. Total density of states $D(E_{\mathrm{F}})$ and projections of the states at the Fermi level E_{F} onto the valence $L_v(E_{\mathrm{F}})$ and conduction bands $L_c(E_{\mathrm{F}})$ of the MgO film for the two-ML MgO/Ag system using the tight-binding method. The states at E_{F} were selected by a Fermi–Dirac smearing function with $kT = 0.1$ eV. The $d = 2.68$ Å system is the fully relaxed interfacial system. The $d = 2.47$ Å is described in the text and has a fixed and reduced MgO/Ag separation. Starting at the third row, the dependence of densities of states and projections is shown when various interfacial matrix elements are set to zero.

System	Zeroed couplings	$D(E_{\mathrm{F}})$ eV^{-1}	$L_v(E_{\mathrm{F}})$ eV^{-1}	$L_c(E_{\mathrm{F}})$ eV^{-1}
$d = 2.47$ Å		0.43	0.028	0.047
$d = 2.68$ Å		0.44	0.029	0.041
$d = 2.68$ Å	Ag_i-Mg_i	0.24	0.0020	0.0033
$d = 2.68$ Å	Ag_i-O_i	0.46	0.051	0.046
$d = 2.68$ Å	Ag_i-$(MgO)_i$	0.25	0.0041	0.0035

TABLE IV. Density of states $L_\alpha(E_{\mathrm{F}})$ projected on the Löwdin orbitals α of the surface atoms for the two-ML MgO/Ag system using the tight-binding method. The states at E_{F} were selected by a Fermi–Dirac smearing function with $kT = 0.1$ eV. The $d = 2.68$ Å system is the fully relaxed interfacial system. The $d = 2.47$ Å is described in the text and has a fixed and reduced MgO/Ag separation. Starting at the third row, the dependence of densities of states and projections is shown when various interfacial matrix elements are set to zero.

System	Zeroed couplings	$L_{\mathrm{O}\,2p_z}(E_{\mathrm{F}})$ 10^{-3} eV^{-1}	$L_{\mathrm{Mg}\,3p_z}(E_{\mathrm{F}})$ 10^{-3} eV^{-1}
$d = 2.47$ Å		1.13	0.66
$d = 2.68$ Å		1.76	0.54
$d = 2.68$ Å	Ag_i-Mg_i	0.36	0.53
$d = 2.68$ Å	Ag_i-O_i	3.73	1.54
$d = 2.68$ Å	Ag_i-$(MgO)_i$	0.07	1.15

and in fact interfering (see below), paths for electronic wave functions to reach the surface. In terms of comparing to computed STM images, however, it is more helpful to consider the projections onto the atomic states on the surface atoms

$$L_{\alpha}\left(E_{\mathrm{F}}\right) = \frac{1}{N_k}\sum_{n,\mathbf{k}} w\left(E_{\mathrm{F}} - E_{nk}\right)\langle\psi_{n\mathbf{k}}|P^{\mathbf{k}}_{\alpha}|\psi_{n\mathbf{k}}\rangle,$$

where $P^{\mathbf{k}}_{\alpha}$ is the projector onto the (Löwdin) atomic orbital α. The second row of Table IV displays these values for the relaxed two-ML MgO/Ag system for the two orbitals that we have found dominate the STM image: O $2p_z$ and Mg $3p_z$ of the surface layer. Both orbitals have weights at E_{F} which correlates with the band projections of Table III and the STM image of Fig. 11(a).

When the MgO/Ag separation is reduced to $d = 2.47$ Å, the resulting two sets of projections are displayed in the first rows of Tables III and IV. The main effect of reducing the separation is to increase the projection onto the conduction band at the expense of the valence band, which in turn significantly increases the projection on the surface Mg $3p_z$ orbital and greatly increases the intensity at the Mg in the STM image Fig. 12(d) at the expense of the O site. This behavior is linked to the enlarged matrix elements between the extended Ag and Mg orbitals upon reduction of their separation.

A final set of manipulations on the system involves selectively removing certain Ag to MgO couplings and observing the result on the electronic structure at E_{F} in the MgO. The third rows of Tables III and IV show the effect or removing (zeroing out) all entries in $H^{\mathbf{k}}_{mi}$ corresponding to orbitals on the interfacial silver atoms, denoted as Ag_i, and all atomic orbitals belonging to the interfacial Mg, denoted as Mg_i. The resulting STM image is shown in Fig. 14(b). Clearly, the interfacial Mg has a strong connection to the Ag as removing these connections makes the projections onto the valence and conduction bands of MgO drop by an order of magnitude while reducing the LDOS at E_{F} on the surface orbitals as well. This explains the dimming of the computed STM image.

However, zeroing the connection from Ag_i to all the orbitals of the interfacial oxygen O_i has a much more complex result. Counterintuitively, the coupling to valence band actually

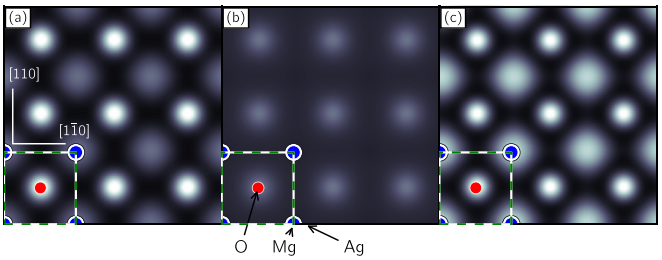

FIG. 14. (Color online) Constant-height LDOS simulations of the two-ML MgO/Ag(001) system based on the atomic-orbital tight-binding model and selective zeroing of the interfacial couplings $H^{\mathbf{k}}_{mi}$: (a) unperturbed Hamiltonian, (b) zeroed Ag_i-Mg_i coupling, (c) zeroed Ag_i-O_i coupling. All images are computed at 1 Å above the surface. The blue (red) circles denote the positions of Mg (O) atoms on the surface layer. The white circles denote positions of Ag atoms at the interfacial layer. The dashed squares outline the unit cells used in the calculations.

increases compared to the pristine case, and the LDOS at E_F on the surface orbitals is greatly enhanced which correlates to STM image becoming brighter than before at both surface atomic sites as seen in Fig. 14(c). When the coupling of Ag_i is zeroed to all orbitals of the interfacial layer $(MgO)_i$, the projections onto the valence and conduction bands are reduced but are above their values when only Ag_i-Mg_i couplings were removed, and the LDOS at E_F of the surface orbitals is greatly reduced for O $2p_z$ but quite large for Mg $3p_z$. These results show interference: zeroing an interfacial connection, Ag_i-O_i, increases projections compared to the pristine case or when zeroing to the entire interfacial layer. There are interfering paths for the propagation of the states at E_F across the interface determined by a complex interplay of Ag-O and Ag-Mg couplings.

We note that there is a complication in our analysis: the Löwdin orthogonalization mixes atomic orbitals around neighboring sites that are coupled by overlap matrix elements, so that zeroing various $H^{\mathbf{k}}_{mi}$ entries is not an extremely spatially localized modification especially given the aforementioned large spatial extent of the Ag and Mg orbitals. The zeroing procedure in the Löwdin procedure is expected to be more insightful in systems with highly localized atomic orbitals.

Summarizing the main findings of this section, the tight-binding approach is useful in that (a) it generates STM images which agree well with the full plane-wave results, (b) it allows one to unambiguously show that the STM image is generated by the electronic structure at E_F on the surface MgO layers, (c) that the MgO/Ag separation d controls the relative importance of Ag-Mg coupling and coupling of the states at E_F to the conduction band of the MgO film, and (d) it illustrates the complex nature of the coupling across the interface and its relation to the formation of the STM image. This coupling across this interfacial system is in fact quite delocalized in real space primarily due to the large spatial extent of the Mg orbitals in the MgO overlayer. We expect similar complex and delocalized behavior at low bias in other metal/oxide interfaces where the key cationic atomic orbitals are large on the scale of the interatomic distances. Conversely, if the cationic atomic states are localized to begin with, e.g., the 3d states of first-row transition metals, the interpretation of the low-bias STM in terms of interfacial behavior may be significantly simplified.

V. SUMMARY

We have investigated the STM contrast at near-zero-bias voltage for thin MgO films on Ag (001) substrates by using DFT first-principles simulations. We found that the STM images cannot be simply and directly attributed to the states of the Ag substrates. The STM image is in fact completely dominated by the contributions of the electronic states of the topmost MgO atomic plane on the surface of the film. Hence, the STM image formation process is as follows: metallic states at the Fermi level originate in the Ag, couple to the MgO atomic orbitals (or the MgO band states) across the interface, propagate through the insulating MgO lattice, and evanescently decay on their way to the surface. The STM image thus is created by the amplitudes of these evanescent states at E_F on the surface atoms. Our results show that the cross-interfacial coupling is complex and long-ranged in this system, defying the simplest nearest-neighbor analysis in terms of contributions solely at short range across the interface. The complex behavior is caused primarily by the large spatial extent of the Mg 3s, 3p, and 3d states that dominate the conduction band of the MgO film. We observed that there are at least two paths for the propagation of the electronic states across the interface, and that they interfere in a complicated manner when forming the STM image above the surface.

In the process of the analysis, we developed a simple tight-binding method that successfully reproduces the STM contrast computed from the more accurate plane-wave calculations. The tight-binding approach permits a variety of analyses to be performed on how the STM image is formed, what information it carries, and the key atomic orbitals that determine its overall behavior. The method is general and applicable to other interfacial systems.

Finally, while this particular interfacial system features delocalized couplings which make simple analysis difficult, the main culprit is the large extent of the cation Mg atomic states that dominate the conduction bands of the MgO. Hence, systems where both the conduction and valence bands of the insulating overlayer are dominated by localized orbitals are preferred: in such a situation, one has a better chance of extracting information on the localized behavior of the buried information from the STM image on the surface. For example, metal oxide films incorporating 3d transition metals should be good candidates for future studies due to the spatial locality of the 3d orbitals.

ACKNOWLEDGMENTS

A.M. acknowledges useful discussions with Matthew S.J. Marshall. This work was supported by NSF MRSEC DMR 1119826 and by the facilities and staff of the Yale University Faculty of Arts and Sciences High Performance Computing Center. Additional computations used the NSF XSEDE resources via Grant No. TG-MCA08X007.

APPENDIX A: BRILLOUIN ZONE INTEGRATION

Since simulated near-zero-bias STM images are computed as LDOS at E_F, we would like to ensure that the position of the Fermi level with respect to critical band edges (such as the MgO valence band) and other features of the density of states is physically robust versus the technical choices made in

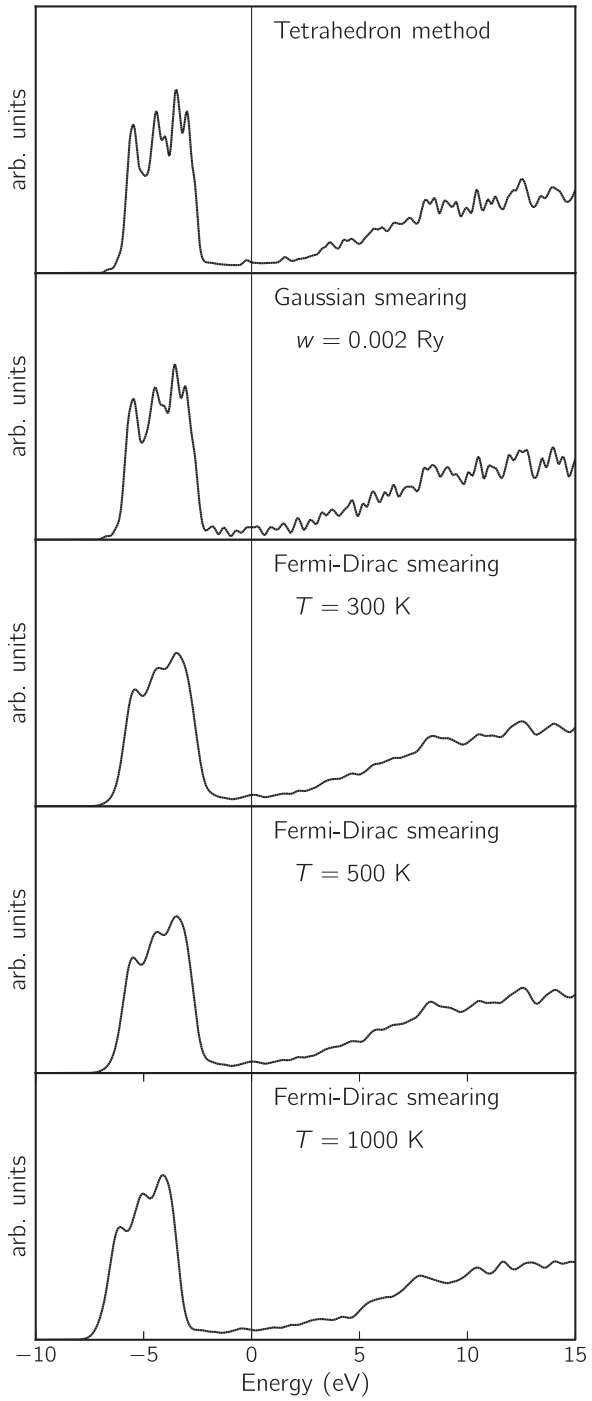

FIG. 15. Density of states for the two-ML MgO/three-ML Ag(001) system computed with various Brillouin zone integration techniques. The Fermi level in each case is indicated by a vertical line at zero energy.

performing the Brillouin zone integrations. Figure 15 shows the density of states for the two-ML MgO/three-ML Ag(001) system, whose structure is shown in Fig. 1, as computed with three different methods: Gaussian smearing with a broadening of 2 mRy, Fermi–Dirac smearing at a variety of temperatures, and the zero-temperature tetrahedron integration method. The figure demonstrates that the density of states and position of the Fermi level are robust to the choice of integration method. We only begin to see slight deviations at the highest temperatures (1000 K) which are not of physical importance in operating STM conditions.

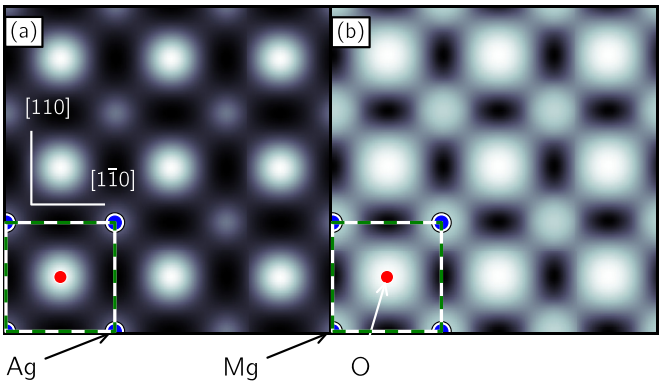

FIG. 16. (Color online) (a) Constant-height and (b) constant-density LDOS at Fermi level for the two-ML MgO/three-ML Ag(001) system. The constant-height image is computed at 1 Å above the surface. The constant-density image is simulated for the density roughly corresponding to the density minimum (darkest region) in panel (a).

APPENDIX B: CONSTANT-HEIGHT VERSUS CONSTANT-DENSITY IMAGES

Figure 16 shows the zero-bias STM simulation (LDOS at Fermi level) of the two-ML MgO/three-ML Ag(001) system shown in Fig. 1. The figure compares the constant-height and constant-density modes. One can see that, qualitatively, the images look quite similar in that the bright spots are at the surface O locations and the dimmer spots are at the surface Mg locations. The main visual difference between the images is due to different contrast ratios.

APPENDIX C: TIP-SURFACE DISTANCE DEPENDENCE IN STM SIMULATIONS

Figure 17 shows the dependence of the simulated constant-height near-zero-bias STM image on the distance from the surface for the two-ML MgO/Ag(001) system. One can see that, while the locations of the main features do not change, there are some changes in the shapes of features. In addition, the quality of images deteriorates with the height increase due to increased numerical noise as discussed in the main text.

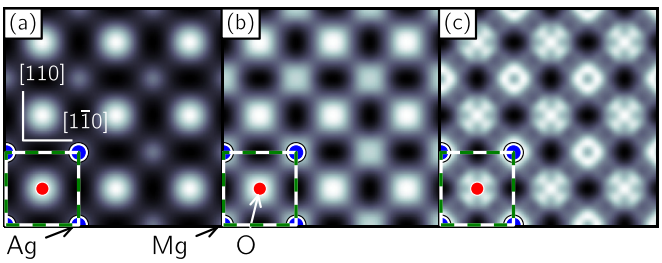

FIG. 17. (Color online) Constant-height near-zero-bias STM simulations of the two-ML MgO/Ag(001) system at (a) 1 Å (b) 2 Å, and (c) 3 Å above the surface.

[1] *Metal Oxide Catalysis*, edited by S. D. Jackson and J. S. J. Hargreaves (Wiley-VCH Verlag, Weinheim, 2009).
[2] *Solid State Gas Sensing* edited by E. Comini, G. Faglia, and G. Sberveglieri (Springer Science, New York, 2009).
[3] P. Zubko, S. Gariglio, M. Gabay, P. Ghosez, and J.-M. Triscone, Annu. Rev. Condens. Matter Phys. **2**, 141 (2011).
[4] E. Y. Tsymbal, E. R. A. Dagotto, C.-B. Eom, and R. Ramesh, *Multifunctional Oxide Heterostructures* (Oxford University Press, Oxford, 2012).
[5] G. Pacchioni and H. Freund, Chem. Rev. (Washington, DC, US) **113**, 4035 (2013).
[6] I. K. Robinson and D. J. Tweet, Rep. Prog. Phys. **55**, 599 (1992).
[7] H. Hashizume, M. Sugiyama, T. Niwa, O. Sakata, and P. L. Cowan, Rev. Sci. Instrum. **63**, 1142 (1992).
[8] E. D. Specht and F. J. Walker, Phys. Rev. B **47**, 13743 (1993).
[9] G. Renaud, A. Barbier, and O. Robach, Phys. Rev. B **60**, 5872 (1999).
[10] M. Gallagher, M. Fyfield, J. Cowin, and S. Joyce, Surf. Sci. **339**, L909 (1995).
[11] S. Schintke, S. Messerli, M. Pivetta, F. Patthey, L. Libioulle, M. Stengel, A. De Vita, and W.-D. Schneider, Phys. Rev. Lett. **87**, 276801 (2001).
[12] N. Lopez and S. Valeri, Phys. Rev. B **70**, 125428 (2004).
[13] J. Tersoff and D. R. Hamann, Phys. Rev. Lett. **50**, 1998 (1983).
[14] J. P. Perdew, in *Electronic Structure of Solids* (Akademie Verlag, Berlin, 1991), p. 11.
[15] D. Vanderbilt, Phys. Rev. B **41**, 7892 (1990).
[16] P. Giannozzi *et al.*, J. Phys.: Condens. Matter **21**, 395502 (2009).
[17] S. G. Louie, S. Froyen, and M. L. Cohen, Phys. Rev. B **26**, 1738 (1982).
[18] L. Bengtsson, Phys. Rev. B **59**, 12301 (1999).
[19] P.-O. Löwdin, J. Chem. Phys. **18**, 365 (1950).
[20] R. W. G. Wyckoff, *Crystal Structures* (Interscience Publishers, New York, 1963–1971).
[21] M. W. Williams and E. T. Arakawa, J. Appl. Phys. **38**, 5272 (1967).
[22] J. P. Perdew, R. G. Parr, M. Levy, and J. L. Balduz, Phys. Rev. Lett. **49**, 1691 (1982).
[23] J. P. Perdew and M. Levy, Phys. Rev. Lett. **51**, 1884 (1983).
[24] C. J. Chen, *Introduction to Scanning Tunneling Microscopy: Second Edition* (Oxford University Press, Oxford, 2008).
[25] L. Giordano, F. Cinquini, and G. Pacchioni, Phys. Rev. B **73**, 045414 (2006).
[26] J. M. Blanco, F. Flores, and R. Pérez, Prog. Surf. Sci. **81**, 403 (2006).
[27] M. Heyde, M. Sterrer, H.-P. Rust, and H.-J. Freund, Appl. Phys. Lett. **87**, 083104 (2005).
[28] H. Galloway, J. Bentez, and M. Salmeron, Surf. Sci. **298**, 127 (1993).
[29] M. Li and E. I. Altman, J. Phys. Chem. C **118**, 12706 (2014).
[30] N. Marzari and D. Vanderbilt, Phys. Rev. B **56**, 12847 (1997).